DOI: 10.61782/fa.2023.0548

forum acusticum 2023

DESIGN OF SOUND ABSORPTIVE METAMATERIALS WITH SHARED WAVEGUIDES BY MEANS OF NUMERICAL ANALYSIS AND ANALYTICAL MODELING

Vidhya Rajendran[1*] **Tomás Méndez Echenagucia**[2] **Andy Piacsek**[3]

[1] Rambol Group, Seattle, United States
[2] Department of Architecture, University of Washington, United States
[3] Department of Physics, Central Washington University, United States

ABSTRACT

Noise can be controlled in naturally ventilated indoor spaces using sound-absorbing panels or ventilated sound barriers. The former has thickness limitations while the latter can be as thick as the exterior wall but requires a specific opening size for air passage. This paper presents a design approach that utilizes the differential evolution algorithm to derive a broadband low-frequency resonator panel. The panels consist of arrays of cells with a central waveguide connecting four Helmholtz Resonators (HRs), and the other end of this waveguide is either closed or open to derive two functionally different resonator panels: a rigidly backed absorption panel and a ventilated sound barrier panel. Three optimization methods are discussed to obtain optimal panel designs: absorption-optimized, impedance-optimized, and phase-optimized. The phase optimization approach is a novel method for panel designs and proved to achieve results comparable to the other two standard approaches. The absorption performance and the transmission loss for rigid-backed and ventilated panels, respectively, are analytically predicted and numerically verified.

Keywords: *acoustic metamaterials, ventilated sound barriers, numerical modeling, analytical methods, sound absorption, transmission loss*

**Corresponding author*: *vidhya.rj28@gmail.com.*

1. INTRODUCTION

Indoor noise pollution in built environments has been increasing in recent years due to a combination of louder sources [1] and a lower use of sound absorption in indoor spaces. More studies are also showing increased evidence regarding the detrimental effects of noisy environments on human activities and health, including an increased incidence of heart disease and impaired cognitive performance [2], as well as higher rates of worker distraction in open office environments [3]. The problem is particularly noticeable in the low-frequency range because sound energy can travel longer distances, and building partitions designed to insulate sound are less effective [4]. Additionally, porous absorption is much less efficient in the lower frequencies and requires a minimum thickness of at least a quarter of the wavelength to be effective.

Building envelopes have many purposes, including serving as acoustic barriers and inlets for natural ventilation. However, in noisy urban environments, minimizing sound transmission into building interiors while allowing fresh air to enter presents a conflicting objective. This often leads building occupants and designers to rely on increased use of mechanical ventilation and HVAC systems instead of natural ventilation to reduce indoor noise, resulting in higher operational emissions due to increased cooling energy demand in our warming climates.

The use of acoustic metamaterials is a promising approach to address the low-frequency noise problem more effectively. Research has demonstrated that resonant absorbers, which incorporate arrays of Helmholtz resonators (HRs) with varying resonant frequencies, can provide effective sound absorption in increasingly broader fre-

quency spectra [5–8]. Additionally, HR arrays can be designed to serve as sound barriers capable of achieving good transmission losses while maintaining open cavities for airflow [9–11]. This type of sound barrier, known as a ventilated sound barrier, is especially suitable for building envelopes as it allows for natural ventilation while reducing the transmission of noise.

This paper presents an approach for designing sound-absorbing panels and ventilated sound barriers that utilize a systematic arrangement of Helmholtz resonator impedances and their phases through analytical modeling and stochastic optimization. The analytical models used are validated by numerical simulations that have previously been calibrated against Impedance tube measurements for the same HR panel designs.

1.1 HR arrays

Certain HR designs do not achieve perfect sound absorption at their resonant frequencies, and these have been called "imperfect" resonators [6]. Although imperfect HRs do not have absorption peaks as high as those of "perfect" HRs, they have broader absorption curves, which means that they perform "imperfectly" over a wider range of frequencies. This allows them to have a higher overlap in frequencies with neighboring HRs of similar resonance frequencies. Previous studies have shown the potential of these designs to achieve good performance over broader frequencies [7, 12]. However, they must be carefully designed to ensure that their mutual interaction increases rather than decreases the overall performance, as discussed in section 1.2.

One example of such HRs is those with embedded necks [5]. This quality can also make them space-efficient, making them particularly suitable for application in buildings. This category can also include designs where the HR necks have a shared opening or waveguide [8]. If the waveguide is only opened to a source room, the resulting HR array can be considered an absorptive panel. If it is opened to both a source and a receiving room, the panel can be considered a ventilated sound barrier, as the opening would allow for the exchange of air between the two sides of the panel. Figure 1 shows a single "cell" containing four HRs that share a waveguide but have different necks, cavity volumes, and resonant frequencies. Each cell is designed with a unique set of 4 neck lengths, 4 neck widths, and 3 angles that define the cavity's shape. This paper uses this "cell" to design absorptive panels and ventilated sound barriers.

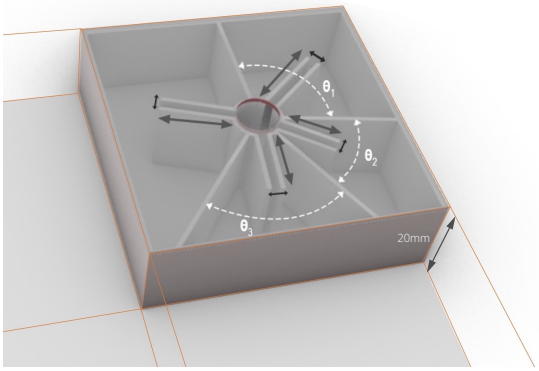

Figure 1. Design of a resonator cell composed of 4 Helmholtz resonators sharing a central channel

1.2 HR cavity phase and mutual interaction

The performance of an array of "imperfect" HRs depends on the interaction between each HR. If the resonant frequencies of neighboring HRs are too different, there will be insufficient overlap, and their combined absorption will not exceed their individual absorption. Additionally, if the sound pressure inside each cavity has the opposite sign, their performance will have a negative effect when combined, reducing the array's performance below that of a single HR. Fig. 2 shows a numerical simulation of a single "cell" with a shared cavity, illustrating the sound pressure for each cavity on the top left and the absorption coefficients on the right. It can be observed that the positive and negative pressures in the two HRs result in an array absorption (solid blue line) that is lower than their single HR's absorption (segmented lines). The impedance of a resonator is calculated by dividing the pressure by its volume velocity. Since these two resonators experience opposing pressures, their surface impedance values oppose each other. Consequently, the opposing impedances cancel out each other, resulting in HRs that negatively impact each other.

2. METHODS

Analytical methods, in conjunction with stochastic optimization, are used to predict the performance of the HR arrays. A numerical model that has previously been calibrated with impedance tube test data is used to validate the results.

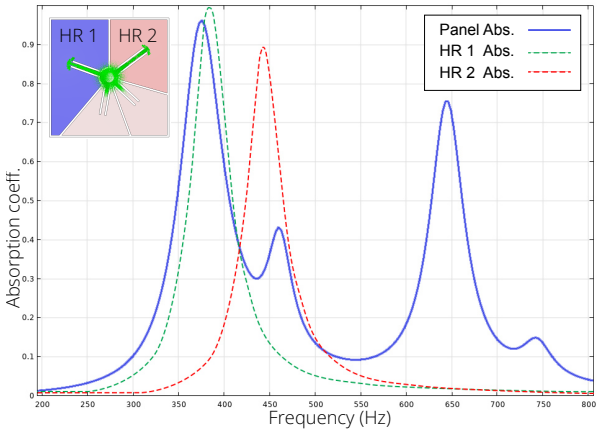

Figure 2. Opposing pressures in the cell's resonator cavities at 460Hz results in reduced absorption quality

2.1 Analytical Methods

Analytical methods are employed to predict the performance of the HR arrays. In both the absorption and transmission cases, the impedances in the necks, cavities, and shared central channels are important in calculating the overall surface impedance of the panel. The impedances in the neck and an arbitrarily shaped cavity are given by Huang et al. [5],

$$Z_{neck} = R_v + R_{rad} + j\rho_t\omega l_n \tag{1}$$

$$Z_{cavity} = \frac{-jS_n\rho_t c_t^2}{\omega V_c} \tag{2}$$

where V_c = (Vol. of cavity - Vol. of embedded neck), and S_n is the area of the neck opening. The complex variables - ρ_t and c_t - denote the complex air density, and the complex sound speed in the neck and cavity tubes. For simplicity, they are assumed to be $\rho_t = 1.25\ kg\ m^{-3}$ and $c_t = 343 + 3.43j$ to account for the losses in the HR [13]. Impedance in the cylindrical central channel,

$$Z_{channel} = j\rho_t c_t cot(k_e L) + j\omega\rho_t L_{corr} \tag{3}$$

where k_e, the effective wavenumber in the channel, is given in [5]. L_{corr} is $0.85\times$radius of the channel.
The viscous losses (R_v) and the radiation losses (R_{rad}) in the neck are given by,

$$R_v = (\frac{l_n}{r} + 2)\sqrt{2\rho_0\omega\eta} \qquad R_{rad} = j\omega\rho_0\delta_n \tag{4}$$

where δ_n, the sum of radiation corrections at either end of the neck, is given in [14].

2.2 Optimization Strategies

This research employs a stochastic optimization algorithm called Differential Evolution (DE) [15], to find the optimal HR cell design, where individual resonators are optimized to work together to produce a constructive performance. A fitness function is used to evaluate different panel designs to determine an optimal performing design. Three different fitness functions are explored that can be used for both absorptive and ventilated panels. Different fitness functions yield different results because each one prioritizes a different parameter.

2.2.1 Fitness 1: Absorption/Transmission Coefficients

The absorption or transmission coefficients of a panel indicate its performance. These dimensionless coefficients are frequency-dependent and range from 0 to 1. For an absorptive panel, a higher absorption coefficient (α) suggests better performance, while for a ventilated panel, a lower transmission coefficient (τ) indicates a quieter interior environment. The fitness function is the area under these graphs. For an absorption panel,

$$\alpha = \frac{4Re[Z_e]}{(1 + Re[Z_e])^2 + (Im[Z_e])^2} \tag{5}$$

For a ventilated panel,

$$T = \frac{2Z_e}{2Z_e cos(k_e L) - j(Z_e^2 + 1)sin(k_e L)}; \quad \tau = |T|^2 \tag{6}$$

where Z_e is the normalized surface impedance of the panel ($\frac{Z_{surf}}{Z_{air}}$).

2.2.2 Fitness 2 - Real and Imaginary parts of surface impedance

The impedance of the panel plays a crucial role in determining its performance, as depicted in Eqn. (5) and Eqn. (6). To achieve maximum absorption, that is $\alpha = 1$, two conditions must be met:

$$Re[Z_{surf}] = Z_{air}; \quad Im[Z_{surf}] = 0 \tag{7}$$

Hence, these conditions are used in the fitness function to derive an optimal performing panel.

2.2.3 Fitness 3 - Phase change in the frequency domain

As shown in section 1.2, opposing phases at a particular frequency in different resonators of the cell can cause destructive performance. To prevent such designs, the phase information (θ) contained in the surface impedance of the panel was used as a fitness function for optimization.

$$\theta = tan^{-1}\left(\frac{Im[Z_{surf}]}{Re[Z_{surf}]}\right) \tag{8}$$

The phase response angle θ is given in radians and ranges from $-\pi/2$ to $\pi/2$. It is called the phase response because it is calculated in reference to the phase of the incoming sound waves (planar waves). The incoming waves vibrate the column of air in the necks of the resonators, producing a radiation response that interacts with the incoming waves. When the phase of the radiation response differs from the phase of the incoming waves, sound energy is lost through the phase-mismatch phenomenon. In the specific case where the phase angle switches from negative to positive at a frequency (i.e., when the phase is 0), the phase response of the panel is exactly opposite to the phase of the source sound waves, which produces a peak absorption at that frequency. The phase fitness function promotes zero-line crossovers from the negative axis and a continual change in the phase angle across the frequency range.

2.3 Numerical modeling

Numerical modeling was employed to validate the predicted performance obtained from the analytical methods. The Pressure acoustics module in COMSOL Multiphysics was utilized for frequency domain simulations. To validate the panel's performance, a standard impedance tube experiment setup was recreated in COMSOL, excluding the microphones. The boundary conditions of the setup include a sound-hard square waveguide boundary enclosing the panel, with plane wave radiation emitted from the front end. Thermoviscous Boundary Layer Impedance conditions were applied to the resonator surfaces to account for losses. For the absorption panel, the emitter and receiver surfaces were placed on the same side, and the reflection coefficient was calculated by integrating the power through these surfaces. In the case of the ventilated panel, the receiver surface was positioned on the opposite side, and a Perfectly Matched Layer (PML) was implemented on the receiver end to prevent additional reflections. The maximum mesh element size was set to $c/f_{max}/8$, where c is the speed of sound in air and f_{max} is the maximum frequency of interest in the simulation.

The numerical and analytical methods used in this paper have been calibrated using data from a standard 2-microphone Impedance tube experiment. The impedance tube was used to measure the normal incidence absorption coefficients for similar HR arrays and a detailed description is provided in [7]. Fig. 3 shows the analytical, numerical, and experimental data comparison for an HR array using the same cell design combined with another resonator type. There is a fairly good agreement between the COMSOL and experimental results. However, the experimental data taper off closer to $800Hz$ because the working frequency range of the Impedance tube is between $100Hz$ and $800Hz$.

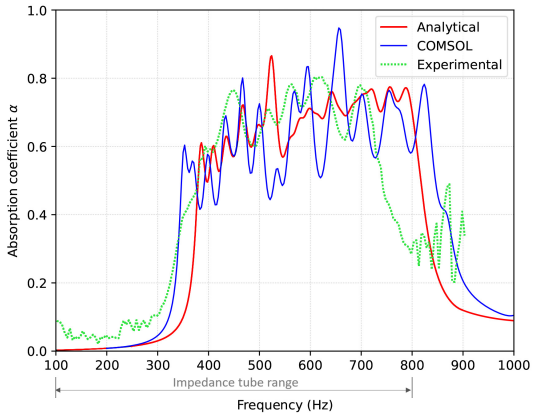

Figure 3. Validation of analytical and numerical results with experimental data from a standard 2-mic Impedance tube setup

3. RESULTS

3.1 Absorption Panels

The absorption coefficient curve of a panel is a reliable indicator of its performance, with higher and wider curves indicating better performance. In this study, the panel depth was limited to $20mm$, as the panel was intended for indoor applications. To compare the different fitness functions, a square panel comprising of 4 resonator cells (or 16 embedded neck resonators), measuring $132mm$ in both length and width, was optimized. The optimal designs generated by the DE solvers demonstrated low-frequency

absorption and broadband behavior within an ultra thin panel.

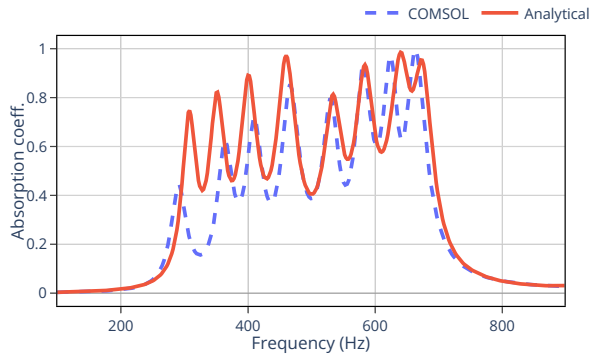

Figure 4. Optimal results with Fitness function 1 - Analytical prediction and Numerical results

Fig. 4 shows the overlapped results of analytical prediction and numerical simulation for a 4-cell panel optimized using the absorption coefficient fitness function (section 2.2.1). This optimization method produced an absorption curve with equally spaced resonant frequencies, which reduces the deeper valleys between the peaks and exhibits a gradually increasing pattern. Because this fitness function optimized the area under the curve, the result exhibits both a broader and taller absorption curve.

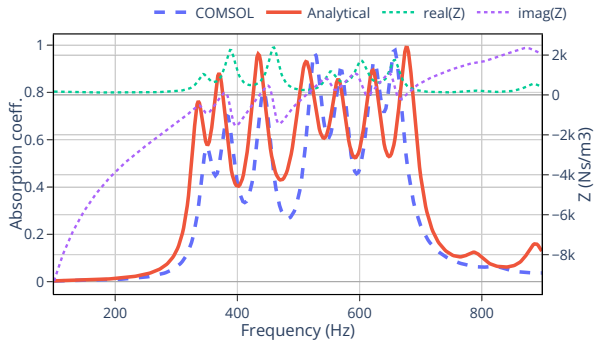

Figure 5. Optimal results with Fitness function 2 - Analytical prediction and Numerical results

The results from the impedance optimization method (section 2.2.2) are shown in Fig. 5, both for analytical prediction and numerical simulation. The conditions (Eqn. (7)) for this fitness function, when satisfied, produce an absorption peak of unity. Therefore, the outcome of this optimization process is a curve with taller peaks but a narrower band of absorption compared to the results from the absorption fitness (see Fig. 4). Clustering of peaks and deeper valleys can be observed in Fig. 5 as a result of prioritizing taller peaks in the impedance fitness function.

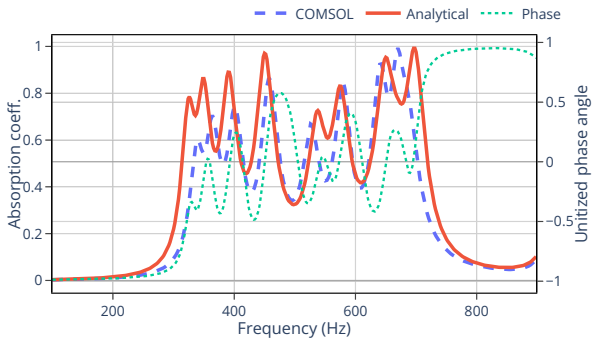

Figure 6. Optimal results with Fitness function 3 - Analytical prediction and Numerical results

Phase-optimized prediction and numerical results are presented in Fig. 6. This graph exhibits both the broad frequency response observed in absorption-optimized results, as well as the taller absorption peaks seen in impedance-optimized results. This function also promotes more overlaps between the resonators (grouping of the peaks) when compared to the equally-spaced result from absorption-optimized. At frequencies where there is no change in phase angle, indicated by a flat line in Fig. 6, there is zero absorption. This occurs before $200Hz$ in the figure. Furthermore, absorption peaks are seen when the phase angle crosses the zero-line from the negative axis to the positive axis, corresponding to a phase angle of π or exactly opposite in phase to the incoming waves.

The phase-optimized design achieves similar performance to the optimal results from the other two methods. The phase function is targeted at designing resonators that do not cause the destructive behavior observed in Fig. 2. Hence, there is a greater overlap between the peaks in Fig. 6. Through mutual interaction, the valleys between the grouped peaks are not deep, while in the absorption-optimized result (see Fig. 4), the valleys between the individual peaks are deep. Therefore, the phase optimization method is very useful for designing a resonator panel with "imperfect" HRs.

3.2 Ventilated sound barriers

The performance of the ventilated sound barriers is evaluated based on two main components - Transmission Loss

(TL) and its opening ratio (ϕ). The TL measures the amount of sound blocked by the panel in decibels (dB), while the opening ratio (ϕ) measures the opening area to the panel's area, which directly impacts the ventilation rate. For the optimization of the ventilated panel design, the same 4-cell panel measuring $132mm \times 132mm$ is used. The maximum depth of the ventilated panel is set at $150mm$ for the DE solvers as these panels are intended to be used on the exterior walls of buildings. This section studies three different opening ratios (15%, 30%, and 45%) to compare their Transmission Loss characteristics. These panels exhibit a reduction of at least $3dB$-$5dB$ in frequencies above $300Hz$, which is perceptible to human ears.

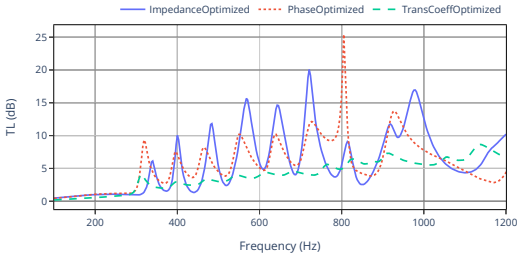

Figure 7. Overlapped TL numerical results for the optimal designs from all the three fitness functions for an opening ratio of 15%

In Fig. 7, the TL numerical results are compared for optimal designs generated using all three fitness functions. These panel designs were optimized for an opening ratio of 15% (equivalent to a $30mm$ opening diameter for the four central channels). The TL curve for the design optimized using the transmission coefficient fitness function is the lowest, with a consistent gradual increase culminating at $6dB$. On the other hand, the impedance-optimized design has a much higher TL with distinctive peak losses ranging from $10dB$ to $20dB$. The performance curve of the phase-optimized design closely matches the profile of the transmission coefficient function's optimal design, but it has about $2.5\times$ the sound loss at the peaks.

The comparative graph in Fig. 8 illustrates the TL numerical results obtained from the three optimization runs for an opening ratio of 30%. As the central channel is wider, the performances have shifted to higher frequencies. The impedance-optimized design exhibits the highest TL at its peaks below $850Hz$, with a small inconsistency around $720Hz$. The phase-optimized design dominates above $850Hz$ as it promotes resonators with overlapping performances. However, this design has its first peak around $500Hz$ while both the other results start at $400Hz$. Once again, in comparison, the transmission coefficient-optimized result displays shorter but consistent peaks.

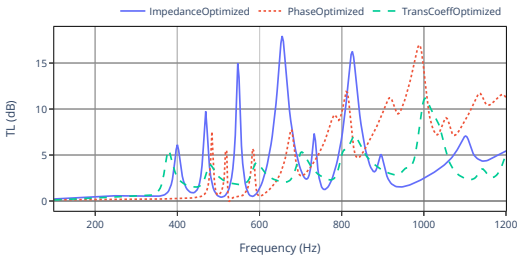

Figure 8. Overlapped TL numerical results for the optimal designs from all the three fitness functions for an opening ratio of 30%

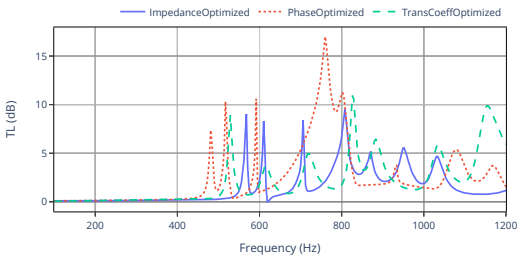

Figure 9. Overlapped TL numerical results for the optimal designs from all the three fitness functions for an opening ratio of 45%

In Fig. 9, the TL performance of optimal designs with a 45% opening ratio is presented. The phase-optimized design exhibits the lowest frequency peak among all the designs, with the first peak around $470Hz$. Additionally, this design displays a high peak sound loss performance, achieving a TL of $10dB$ over an $80Hz$ bandwidth between $700Hz$ to $800Hz$. This is due to the phase opti-

mization method promoting overlapping of resonator performances compared to other methods, resulting in wider peaks. On the other hand, the impedance-optimized design, while lacking a broadband performance, has consistent peaks. In this case, the transmission coefficient-optimized and impedance-optimized designs show comparable performances.

The opening ratio directly impacts the frequency bandwidth of performance and the height of the peaks. As the openings become wider, the panels exhibit reduced transmission loss performance, and their performance is shifted towards higher frequencies.

3.3 Ventilation rate

The primary objective of ventilated panels is to allow for natural airflow, which is driven by the buoyancy effect resulting from differences in air temperature between the indoors and outdoors. The amount of natural ventilation achieved is measured by the ventilation rate, q in (m^3/s) [11],

$$q = AC_d\sqrt{\frac{\Delta T g h}{(T_1 + 273)}} \tag{9}$$

where A is the area of each opening, C_d is the discharge coefficient (typically 0.6) [11], T_1 the internal temperature, ΔT difference between the internal and external air temperatures, g is the gravitational force, and h is the height between the openings.

All variables in Eqn. (9), except for A, remain constant for designs with different opening ratios. Thus, the ventilation rate is affected only by the opening area, and hence, the opening ratio. Therefore, higher opening ratios lead to better natural ventilation. However, as shown in Fig. 10, increasing the opening ratio lowers the transmission loss performance of the panel.

4. DISCUSSION AND CONCLUSION

This study proposes three optimization strategies that produced optimal designs for both absorption and ventilated panels using analytical methods. The first strategy, absorption or transmission coefficient optimization (described in section 2.2.1), is a traditional method for optimizing the HR array for a specified frequency bandwidth. The second method, impedance-based fitness function (discussed in section 2.2.2), uses established conditions to achieve a high-performing panel. The third approach uses phase information for optimization, as described in section 2.2.3. This is a novel approach for designing both absorption and ventilated panels. The optimal designs produced using this approach were compared to designs generated using the other two standard methods, and the results were comparable. Notably, in the case of absorption panels, the phase optimization method promoted designs where the individual resonator performances overlapped to produce a higher absorption peak. The same behavior is observed in the phase-optimized ventilated panel with an opening ratio of 45% (Fig. 9). Therefore, this method is a powerful approach for designing a resonator array with "imperfect" HRs that can exhibit good overall performance.

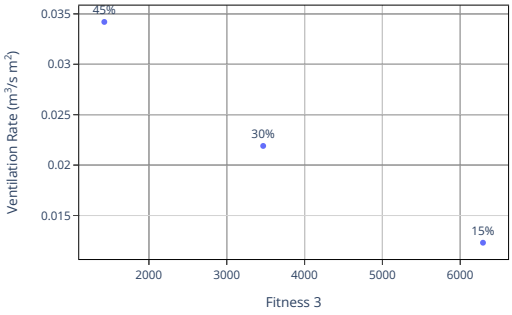

Figure 10. TL performance vs. Ventilation Rate for the three opening ratios

The thin and compact absorption panel designs generated in this research show broadband and good performance in low frequencies. To extend the panel's performance to frequencies below $300Hz$, some of the 4-resonator cells can be swapped with 3-resonator cells where the cavities have more room to absorb very low frequencies within the same panel depth. A similar approach cannot be applied to ventilated panels. Increasing the opening ratio shifts the performance of the ventilated panels to higher frequencies due to the lack of space for longer necks, which absorb most of the sound loss through viscous losses. To improve ventilated panel's performance at lower frequencies, a folded neck design is necessary.

The analytical predictions in this research were supported by numerical simulations, which closely matched the COMSOL results (refer to section 3.1). Although there are no experimental data available to validate the numerical results presented in this research, the authors

used a calibrated model for the analytical and numerical modeling. This calibration was done based on the experimental data from standard Impedance tube measurements (see Fig. 3).

The designs presented in this research exhibit high peaks and valleys in their performance, which could be improved by incorporating multiple "imperfect" resonators operating within the same frequency range. To achieve this, the dimensions of the panel can be increased to $200mm \times 200mm$, allowing for the integration of 9 resonator cells, or 36 HRs. The authors were able to achieve broadband absorption using a $200mm \times 200mm$ panel composed of cylindrical HRs and have presented this design in their paper [7].

5. FUTURE WORK

Future work will involve the study and optimization of the ventilation capabilities of sound barriers using computational fluid dynamics, as well as their laboratory testing in acoustic transmission suites and wind tunnels. Additionally, the design and optimization process will be refined to include fabrication constraints and geometric simplifications to enable mass production.

6. REFERENCES

[1] M. S. Hammer, T. K. Swinburn, and R. L. Neitzel, "Environmental noise pollution in the united states: Developing an effective public health response," *Environmental Health Perspectives*, vol. 122, no. 2, pp. 115–119, 2014.

[2] S. Stansfeld and M. Matheson, "Noise pollution: non-auditory effects on health," *Br Med Bull*, vol. 68, pp. 243–257, 2003.

[3] S. Abbaszadeh, L. Zagreus, D. Lehrer, and C. Huizenga, "Occupant satisfaction with indoor environmental quality in green buildings," 2006.

[4] S. Kumar and H. P. Lee, "The present and future role of acoustic metamaterials for architectural and urban noise mitigations," *Acoustics*, vol. 1, no. 3, pp. 590–607, 2019.

[5] S. Huang, X. Fang, X. Wang, B. Assouar, Q. Cheng, and Y. Li, "Acoustic perfect absorbers via helmholtz resonators with embedded apertures," *The Journal of the Acoustical Society of America*, vol. 145, no. 1, pp. 254–262, 2019.

[6] S. Huang, Z. Zhou, D. Li, T. Liu, X. Wang, J. Zhu, and Y. Li, "Compact broadband acoustic sink with coherently coupled weak resonances," *Science Bulletin*, vol. 65, no. 5, pp. 373–379, 2020.

[7] V. Rajendran, A. Piacsek, and T. Méndez Echenagucia, "Design of broadband Helmholtz resonator arrays using the radiation impedance method," *The Journal of the Acoustical Society of America*, vol. 151, pp. 457–466, 01 2022.

[8] S.-H. Baek, J.-Y. Jang, K.-J. Song, and S.-H. Park, "Design of flat broadband sound insulation metamaterials by combining helmholtz resonator and fractal structure," *Journal of Mechanical Science and Technology*, vol. 35, no. 7, pp. 2809–2817, 2021.

[9] X. Wang, X. Luo, B. Yang, and Z. Huang, "Ultrathin and durable open metamaterials for simultaneous ventilation and sound reduction," *Applied Physics Letters*, vol. 115, 10 2019. 171902.

[10] S. Kumar, T. B. Xiang, and H. P. Lee, "Ventilated acoustic metamaterial window panels for simultaneous noise shielding and air circulation," *Applied Acoustics*, vol. 159, p. 107088, 2020.

[11] G. Fusaro, X. Yu, J. Kang, and F. Cui, "Development of metacage for noise control and natural ventilation in a window system," *Applied Acoustics*, vol. 170, p. 107510, 2020.

[12] S. Huang, X. Fang, X. Wang, B. Assouar, Q. Cheng, and Y. Li, "Acoustic perfect absorbers via spiral metasurfaces with embedded apertures," *Applied Physics Letters*, vol. 113, no. 23, p. Article 233501, 2018.

[13] J. Li, W. Wang, Y. Xie, B.-I. Popa, and S. A. Cummer, "A sound absorbing metasurface with coupled resonators," *Applied Physics Letters*, vol. 109, no. 9, p. 091908, 2016.

[14] V. Romero-García, G. Theocharis, O. Richoux, and V. Pagneux, "Use of complex frequency plane to design broadband and sub-wavelength absorbers," *The Journal of the Acoustical Society of America*, vol. 139, no. 6, pp. 3395–3403, 2016.

[15] R. Storn and K. Price, "Differential evolution–a simple and efficient heuristic for global optimization over continuous spaces," *Journal of global optimization*, vol. 11, no. 4, pp. 341–359, 1997.